Original Research Article

Bathymetric modelling for long-term monitoring of water dynamics of Ramsar-listed lakes using inundation frequency and photon-counting LiDAR data

Zhenyu Zhang [*], Xiaoye Liu

School of Surveying and Built Environment, University of Southern Queensland, Toowoomba, Queensland 4350, Australia

ABSTRACT

Accurate information on lake bathymetry and water dynamics is crucial for comprehending the intricate ecological processes in wetland ecosystems, which in turn can inform effective conservation and management strategies. However, obtaining such information can be challenging, particularly in remote areas with limited data. This study presents a way to leverage inundation frequency and ICESat-2 photon-counting LiDAR data to develop bathymetric models for Ramsar-listed lakes in a semi-arid region of Australia. Based on developed bathymetric models, monthly time series of water areas, levels and volumes were derived, providing a long-term view of the water dynamics of the two lakes from1987-2021. This is the first time that such detailed bathymetry and long-term water dynamics have been established for Ramsar-listed lakes in Australia's Outback. The findings of this study provide the most up-to-date information on the long-term trends of the Ramsar-listed lakes in the region and highlight the lakes' prolonged dry spells when drought conditions prevailed through much of the 2000s and the 2010s as denoted by rainfall deficiencies and high evaporation. The outcome of this study serves as a valuable baseline for understanding the historical and ongoing status of these Ramsar-listed lakes in a warming and drying climate and contributes to the development of strategic plans to fulfill international obligations for wetland protection under the Ramsar Convention.

1. Introduction

Lake bathymetry which describes the water depth or underwater topography of a lake is critical information for hydrological, ecological, and geomorphological research and applications (Dörnhöfer and Oppelt, 2016; Fassoni-Andrade et al., 2020; Heathcote et al., 2015; Hollister et al., 2011; Khazaei et al., 2022). It plays an important role in water dynamic monitoring, water balance determination, ecohydrological modelling, climate change assessment, and wetland conservation (Messager et al., 2016; Mishra et al., 2010; Mohammed and Tarboton, 2011). However, lake bathymetric models are either unavailable or difficult to get (Heathcote et al., 2015; Messager et al., 2016), particularly in remote areas with limited data. Bathymetry is traditionally mapped using echo-sounding equipment on a boat. The echo-sounding method can produce accurate depth profiles along transects, but it is inefficient and expensive (Gao, 2009). It is also not feasible to measure shallow and episodical lakes, particularly in dry periods (Abdallah et al., 2013; Armon et al., 2020; Leon and Cohen, 2012). Airborne bathymetric LiDAR (light detection and ranging) is an efficient method for underwater

---

Please cite this article as: Zhenyu Zhang, Xiaoye Liu, *Ecohydrology & Hydrobiology*, https://doi.org/10.1016/j.ecohyd.2023.10.003

terrain measurement. This method can measure water depth up to tens of metres or two to three times the Secchi depth, but it is relatively expensive (Gao, 2009; Mader et al., 2021). By comparison, satellite derived bathymetry (SDB) from multispectral or hyperspectral imagery has proven to be a cheaper and more spatially extensive method for bathymetric mapping (Hodúl et al., 2018). Nevertheless, the major drawback of most SDB methods requires in-situ water depth data for model construction. This requirement precludes the applications of SDB methods in regions where in-situ depth data is unavailable (Forfinski-Sarkozi and Parrish, 2019; Gao, 2009). Furthermore, the measurable depth of the SDB methods is affected by the water turbidity (Gao, 2009). Fortunately, it has been shown that satellite laser altimetry data from NASA's Ice, Cloud, and land Elevation Satellite (ICESat) missions offer great opportunity to model inland water bathymetry.

Compared to radar altimetry data, the ICESat-2 mission has small footprints and high accuracy and offers greater opportunity to measure inland water bodies (Zhang et al., 2022). ICESat-2 which was launched in September 2018 carries the first spaceborne photon-counting LiDAR, the Advanced Topographic Laser Altimeter Systems (ATLAS). The ICESat-2 mission acquires data along 1,387 reference ground tracks (RGTs) with a 91-day repeat cycle. The observatory position, attitude, travel time of individual photon determined from the ALTAS produce a geolocation for each photon (Neumann et al., 2019). However, the LiDAR points alone are not dense enough to create bathymetry models. Therefore, other spatial datasets, e.g., inundation frequency are needed to interpolate the gaps between the ICESat-2 measurements for modelling the bathymetry of inland water bodies.

Inundation frequency (or referred to as flood frequency or water occurrence) is the number of times an area is flooded in a given period (Fassoni-Andrade et al., 2020; Park et al., 2020; Pekel et al., 2016). For a lake or reservoir, higher inundation frequency corresponds to a lower elevation in the lake floor while lower inundation frequency corresponds to a higher elevation. Within a water dynamic area, locations with a same inundation frequency value should theoretically have a same elevation for the terrains in these locations (Li et al., 2020). Therefore, relative height differences in the water dynamic area can be determined from an inundation frequency dataset. If absolute elevations based on an orthometric height datum are available and cover all the inundation frequency values in the area, a bathymetric model can be generated for the water dynamic area by allocating the absolute elevations to the corresponding inundation frequency values (Li et al., 2021). Xu et al. (2022) created a bathymetry map within the water dynamic area of Lake Mead using water occurrence data derived from Landsat images and ICESat-2 data. However, the bathymetric map can only be produced within the lake water dynamic area. For an area with permanent water occurrence, the bathymetry cannot be created using proposed method (Fassoni-Andrade et al., 2020). Similar method has been used by Armon et al. (2020) to derive bathymetric maps for three ephemeral desert lakes. However, it should be noted that the desert lakes usually filled very occasionally from rare episodic floods and were dry for most of the time. For example, Lake Eyre in central Australia, one of the study areas in Armon et al. (2020) rarely fills with water and is most often empty, with fully (or nearly fully) filling about once every two decades (Kotwicki and Allan, 1998; Leon and Cohen, 2012; May et al., 2022; Prata, 1990). Therefore, the inundation frequency values in such an infrequent inundation area are very likely to compromise the dependability of the derived lake bathymetry. Thus, inundation frequency information is more appropriate for creating lake bathymetric models in semi-arid regions where water levels in lakes change frequently.
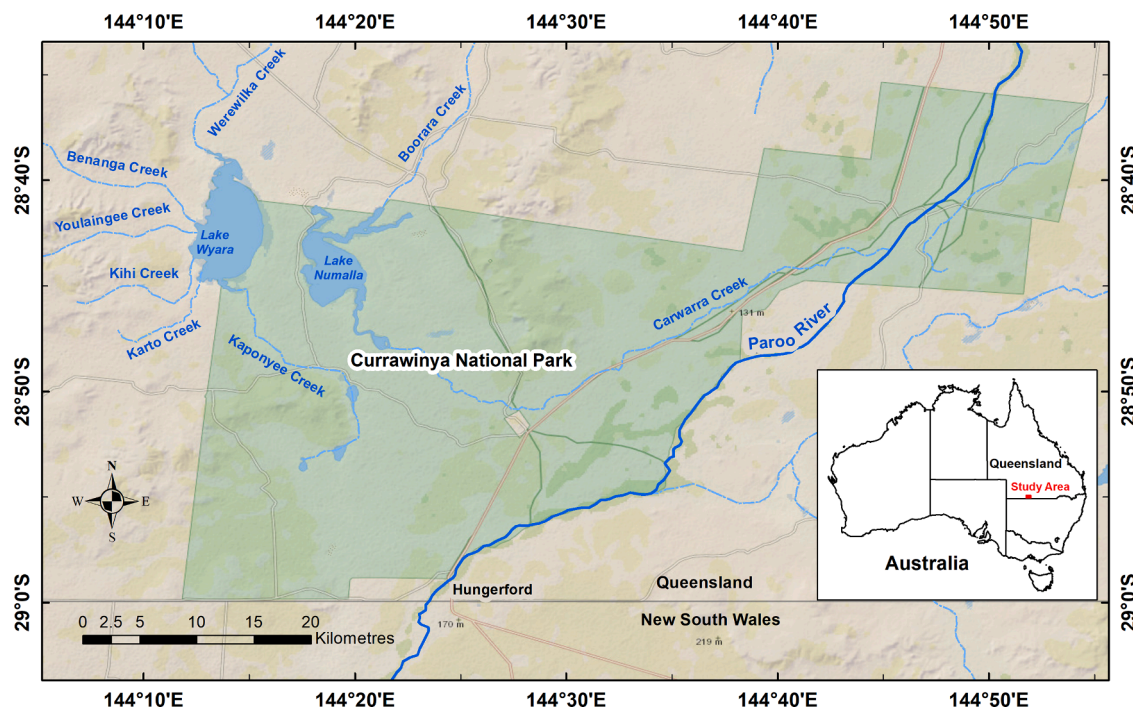

Fig. 1. Study area map showing Lake Wyara and Lake Numalla in Currawinya Lakes Ramsar site, southwest Queensland, Australia. Background shows base map from Environmental Systems Research Institute (ESRI).

Both application examples as mentioned above used ICESat-2 ATL03 data to extract elevations in the lake floors (Armon et al., 2020; Xu et al., 2022). The ATL03 data is an ATLAS level 2 product which provide heights above the WGS84 ellipsoid (ITRF2014 reference frame), latitudes, longitudes and time for individual photons (Neumann et al., 2019). The individual photon points can penetrate water up to several metres. The individual photon points could be returned from the water surface, underwater topography (in shallow water) and background noises. Therefore, the ATL03 data contains both signal and noise points. Detection of the signal points from the noisy ATL03 data is time-consuming and is likely to increase the uncertainty of derived bathymetry. ICESat-2 ATL08 Land and Vegetation Height product should be used to obtain more reliable terrain heights of lake floors than the ATL03 data in the generation of the bathymetry (Cooley et al., 2021; Ryan et al., 2020). Once the bathymetric model is accurately created, a hypsometric curve describing the relationship between water surface area and level (or elevation) (E-A relationship) for the lake can be directly derived from the bathymetry. Some other key parameters of the lake, such as water depth, volume and their variations can subsequently be derived from the lake bathymetry and the hypsometric curve (Bacalhau et al., 2022; Li et al., 2020; Liu and Song, 2022; Messager et al., 2016; Zhang et al., 2022).

This study aims to develop accurate bathymetric models for monitoring the long-term water dynamics of Ramsar-listed lakes in semi-arid Australia by leveraging the inundation frequency and ICESat-2 photon-counting LiDAR data. The specific objectives are: a) to examine the feasibility of combining the inundation frequency and the photon-counting LiDAR data to produce thorough bathymetric models of the lakes in semi-arid region of Australia with limited data availability; b) to determine long-term water dynamics in the lakes to comprehend the historical and ongoing status of Ramsar-listed lakes in a warming and drying climate; and c) to gain new insight into long-term water dynamic trends in Ramsar-listed lakes to help understand the complex ecological interactions in wetland systems and support the fulfillment of international obligations for wetland protection under the Ramsar Convention.

2. Materials and Methods

2.1. Study Area

Currawinya Lakes Ramsar site is in the Paroo River Catchment within the northern Murray-Darling Basin in southwest Queensland, Australia. The boundaries of the Ramsar site are generally coincident with those of Currawinya National Park (Fig. 1), covering an area of 1513 km^2 (NPRSR, 2014). The Ramsar site is a mosaic of a river, alluvial plains, large and small lakes, claypans, springs, creeks, and waterholes. It has some of the most diverse wetland types in the Australian Outback, with largely unmodified permanent and intermittent saline and freshwater wetlands (QDEHP, 2014). The two largest water bodies within the Ramsar site, Lake Wyara and Lake Numalla, are only about 3 km apart (Fig. 1) but are distinctively different and have different catchments (Kingsford and Porter, 1994; QDEHP, 2014).

Lake Wyara, a saline lake, fills from its own closed catchment, receiving most of its inflows from Werewilka Creek at the northern
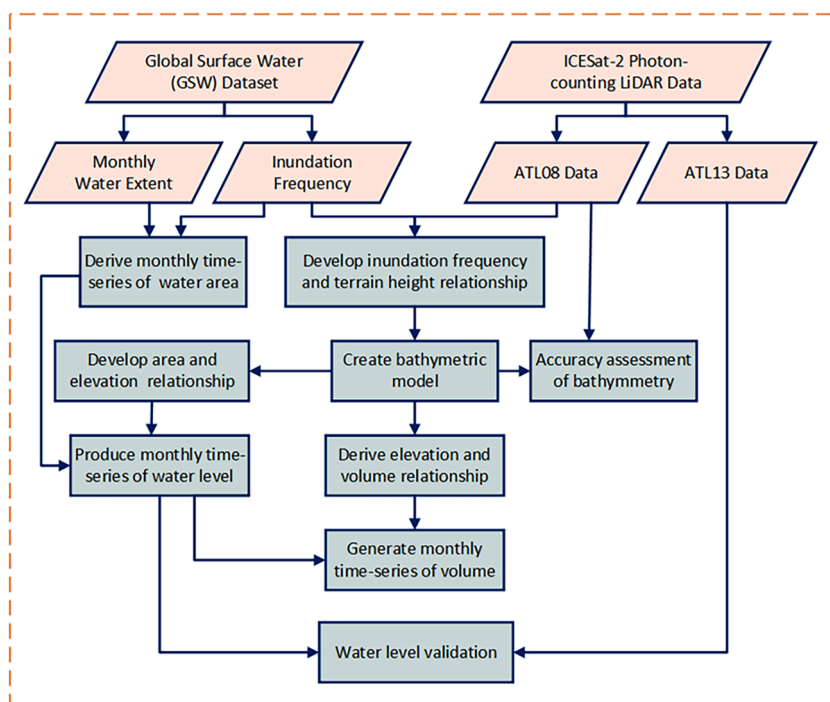

Fig. 2. Methodology flowchart showing the input data and processing procedures in this study.

end (Timms, 2001, 2006), but also from other creeks in the adjacent uplands to the west which include the Benanga, Youlaingee, Kihi and Karto as shown in Fig. 1 (Biggs et al., 2010; Kingsford and Porter, 1994). It occasionally receives floodwaters from the Paroo River via Kaponyee Creek to the south (Fig. 1) and then the water flowbacks as the flood level drops on the Paroo floodplain (Timms, 1998, 2006). Lake Numalla, on the other hand, is a freshwater lake, lying near edge of the Paroo River floodplain along Boorara Creek and being connected to the Paroo River by a distributary channel of Carwarra Creek (Timms, 2006). It fills primarily from Boorara Creek to the north, but also from the Paroo River via Carwarra Creek during floods (Fig. 1) (Biggs et al., 2010; Timms, 2006). Both lakes were classified as permanent lakes (NPRSR, 2014), but were dry during extreme drought (Timms, 2006).

The Currawinya Lakes Ramsar site, situated within a semi-arid climatic region, has a very hot and dry climate with a marked austral summer rainfall pattern (average 285.7 mm per annum, with an average of 41.3 mm in January and 12.5 mm in September) and high average temperatures. Long term average rainfall has remained relatively constant, despite significant inter-annual variability (QDEHP, 2014). The average minimum temperature is 24°C and maximum is 37°C in January, and the average temperature in July is from 6°C to 20°C. Evaporation rates are very high in comparison to rainfall. The average evaporation is about 2000 mm per annum (QDEHP, 2014). The lakes are characterised as hydrologically closed lakes with a high degree of hydrological variability. The water levels of the lakes are controlled by local rainfall, evaporation, and occasional flood inflows from the Paroo River (QDEHP, 2014; Timms, 2006). The Paroo River Catchment is influenced by summer monsoon rainfall, so the river flows are irregular but floods within the Ramsar site are typical during austral summer and/or autumn months (QDEHP, 2014).

2.2. Data and methods

The flowchart as shown in Fig. 2 describes the input data and the methodological procedures undertaken in this study. The procedures include the major steps as follows: a) develop relationship between inundation frequency and terrain height; b) create bathymetric model; c) develop hypsometric relationship between water surface area and level; d) derive monthly time-series of water area; e) produce monthly time-series of water level; f) derive relationship between water level and volume; generate monthly time-series of water volume; and g) accuracy assessment and validation. Details are presented in the following sections.

2.2.1. Inundation frequency and monthly water history data

Global Surface Water (GSW) dataset (Pekel et al., 2016) was extracted from https://developers.google.com/earth-engine/datasets/catalog/landsat using Google Earth Engine (GEE), a cloud-based computing platform (Gorelick et al., 2017). The GSW dataset has been developed in the framework of the Copernicus Programme from Landsat satellite imagery by European Commission's Joint Research Centre. The GSW dataset was initially created from the archive of the Landsat 5 Thematic Mapper (TM), Landsat 7 Enhanced Thematic Mapper Plus (ETM+) and Landsat 8 Operational Land Imager (OLI) data acquired between March 1984 and October 2015 using expert system in GEE (Pekel et al., 2016). The GSW dataset quantifies the distribution and spatiotemporal variations of the Earth's surface water at a 30 m spatial resolution between 1984 and 2015 (recently, it has been updated to 2021). It contains many sub-datasets to illustrate different facets of the spatial and temporal distribution of the surface water over the 38 years. Two sub-datasets, Surface Water Occurrence (SWO) and Monthly Water History (MWH) data were extracted from the GSW dataset for use in this study. For details of other sub-datasets in the GSW dataset, please refer to Pekel et al. (2016). The SWO data represent the frequency of occurrence of water in each pixel from March 1984 to December 2021, which was calculated as the ratio (in percentage ranging from 0% to 100% with an interval of 1%) of the times classified as water versus the total valid observations over the 38/ years. To overcome the possible biases caused by temporal distribution of the valid observations, i.e., more cloud-free observations available during dry seasons than wet seasons, the water occurrence data were calculated by Pekel et al. (2016) at a month-by-month time step which was intended to normalise the occurrence against seasonal variation in the number of valid observations across the year. Long-term overall SWO data were then obtained by averaging the monthly water occurrence results (Pekel et al., 2016). Over a lake or reservoir, the water occurrence is usually referred to as inundation frequency. Therefore, from hereon, the SWO is called inundation frequency in this study. The inundation frequency value of each pixel in a lake area changes with the water level variations over time. For example, pixels with 100% inundation frequency show locations with permanent water presence while 0% being pixels which have never been detected as water. Other occurrence values represent pixels which are inundated on an episodic basis. Simply put, a higher percentage value of inundation frequency corresponds to a lower terrain elevation while a lower percentage value corresponds to a higher terrain elevation. Consequently, the distributions of inundation frequency values over a lake area can be considered as a kind of "terrain model" of the lake topography but without elevation or height values. If the relationship between the inundation frequency values and the terrain elevations in a height datum is established, a bathymetric model or terrain model for the lake can be generated (Li et al., 2021).

The MWH data provide monthly water extents in which each pixel was classified as "water", "not water" or "no data". Here, the MWH data (available from 1987 to 2021 in the study area) were extracted for Lake Numalla and Lake Wyara, representing monthly time series of water areas of the two lakes over the 35 years. It should be noted that because of the impacts of clouds, cloud shadows, terrain shadows, and the Landsat 7 scanline corrector (SLC) failure since May 2013, contaminated pixels have been classified as "no data" in the GSW dataset, leading to underestimated water surface areas of the lakes. To overcome this problem, we adopted a method proposed by Zhao and Gao (2018) to create improved water areas of the lakes by automatic correction of contaminated pixels in the MWH data using the inundation frequency data. This method is predicated on the premise that for pixels classified as water with a same specific inundation frequency value, all contaminated pixels (classified as "no data") which have inundation values greater than or equal to that specific inundation frequency values were rectified from "no data" to "water" (Zhao and Gao, 2018). In this way, improved monthly water extents (or monthly time-series of water area) of the Lake Numalla and Lake Wyara from March 1987 to 2021

were produced.

2.2.2. ICESat-2 data

The ATLAS splits a single outgoing laser pulse into 3 pairs of photon-counting beams (approximately 3.3 km apart between pairs) for surface profiling at a 10kHz pule rate. Each pair, labelled with a ground track (GT) number, consists of a high energy (about 100 mJ) beam (strong beam) and a low energy (25 mJ) beam (weak beam). The strong and weak beams in each pair are separated by about 90 m in the across track direction, with an approximately 17 m diameter footprint on the ground. The ICESat-2 orbits the Earth at 496 km height with an instrument pulse rate of 10 kHz and the nominal ground speed of about 7000 m/s, resulting in a nominal 0.7 m along track point spacing (Neumann et al., 2019).

Both ICESat-2 ATL08 Land and Vegetation Height product (Version 5) (Neuenschwander et al., 2021b) and ATL13 Along Track Inland Water Data (Version 5) (Jasinski et al., 2021b) were downloaded from https://openaltimetry.org/data/icesat2/ for this study. The ATL08 and ATL13 are the two datasets of many surface-specific and higher-level products developed from ATL03 data (an ATLAS level 2 product) (Neumann et al., 2021b) which provide heights above the WGS84 ellipsoid (ITRF2014 reference frame), latitudes, longitudes, and time for individual photons (Neumann et al., 2021a; Neumann et al., 2019). The ATL03 product is the single data source for all photon data and ancillary information needed by higher-level ATLAS/ICESat-2 products, such as ATL08 and ATL13. The ATL08 product provides mean WGS84 ellipsoidal height and statistic information for terrain and canopy surfaces in a fixed segment size of 100 m along the ground track (Neuenschwander et al., 2021a). The ATL13 data product provides mean water surface height (orthometric height based on EGM2008) and descriptive statistics for inland water bodies in individual segments along-track for each ATLAS beam. The length of segment varies, determined by the distance along track to aggregate 100 signal photons (Jasinski et al., 2021a). More details about the ATL08 and ATL13 products please refer to Neuenschwander and Pitts (2019), Neuenschwander et al. (2021a) and Jasinski et al. (2021a).

2.2.3. Climate data collection and compilation

Local climate data including rainfall and evaporation were obtained from the meteorological data stored in the SILO data drill dataset (www.longpaddock.qld.gov.au/silo/). SILO is a Queensland Government database containing continuous daily climate data for Australia from 1889 to present. Gridded datasets on a 0.05° by 0.05° spatial resolution were constructed using observed climate data provided by the Australian Bureau of Meteorology (Jeffrey et al., 2001). Daily rainfall and Class A pan evaporation were downloaded from grided datasets in 12 grid cells (Fig. S1) related to Lake Wyara and Lake Numalla. The climatic conditions of the study area were represented by averaging the data from 12 grid cells. Monthly rainfall and evaporation data were then calculated from averaged daily data.

2.2.4. Bathymetry modelling

To derive the lake bathymetry (or topography), the ATL08 data returned from lake terrains (not from water surface) should be used. Ideally, the ATL08 data obtained during a period when the lake was dry would be able to fully describe the lake bathymetry (or the topography of the lake floor). In the Currawinya Lakes Ramsar site, both Lake Wyara and Lake Numalla were dry in 2019 and in the first two months of 2020. Therefore, the available ATL08 data in February and August 2019 and in February 2020 over the two lakes were extracted for bathymetric modelling and model validation. Details are listed in Table 1. The ATL08 data acquired in 2019 were used to model the bathymetry of the two lakes, and the data in 2020 were used for accuracy assessment of derived bathymetric models. The shores of the semi-arid lakes exhibit a scattering of low shrubs (QDEHP, 2014). To mitigate the potential influence of the vegetation canopy on bathymetry generation, visual checks were conducted to exclude the ATL08 segments returned from the shrubs.

The ATL08 data were first overlaid on the inundation frequency image of the two lakes (Fig. S2). The ATL08 data were then paired with the inundation frequency pixels. To remove the outliers of the ATL08 data, elevations greater than three standard deviations from mean of elevations corresponding to a specific inundation frequency value were discarded. Visual checks were also undertaken to further remove any spurious outliers. The terrain elevation was then obtained as the mean of the ATL08 data corresponding to the specific inundation frequency value. The elevations of the ATL08 data were converted to the Australian Height Datum (AHD) to depict the terrain heights of lake floors. The relationships between the inundation frequency and the terrain height were established by polynomial functions for the two lakes (see Section 3.2).

The inundation frequency ranges from 1% to 82% and 1% to 66% for Lake Wyara and Lake Numalla respectively. The ATL08 data cover all ranges of the inundation frequencies for Lake Numalla, so all the pixels in the inundation frequency image were allocated an elevation value from corresponding ATL08 data. For Lake Wyara, the ATL08 data cover most part of the inundation frequencies (from 1% to 62%). The pixels within this range of the inundation frequencies were directly allocated elevations from corresponding ATL08

Table 1

ICESat-2 ATL08 data used for bathymetry modelling and validation, including reference ground track (RGT) ID, ground track (GT) number and acquisition date.

RGT Number	GT Number	Date	Usage
RGT 703	GT1 and GT2	13 Aug. 2019	Bathymetric modelling for Lake Wyara
RGT 939	GT2 and GT3	27 Feb. 2019	Bathymetric modelling for Lake Numalla
RGT 703	GT3	10 Feb. 2020	Model validation of Wyara
RGT 703	GT1	10 Feb. 2020	Model validation of Numalla

data. Elevations for pixels with the inundation frequency values from 63% to 66% were extrapolated from the regression equation between the inundation frequency and the ATL08 terrain height. Once all the pixels in the inundation frequency images were allocated ICESat-2 elevations, the complete bathymetric models with 5 m horizontal resolution were generated for the two lakes. In the above procedure, bilinear interpolation is employed to refine the horizontal resolution of the SWO data from 30 m to 5 m to create the bathymetric models with higher horizontal resolution. Both Lake Wyara and Lake Numalla are characterised by a flat lakebed and steep bank (as shown in Section 3.4). The bathymetric models with enhanced resolution can better represent the abrupt elevation changes along the banks and shorelines, ensuring the effective capture and visualisation of these distinctive features.

2.2.5. Water dynamic modelling

Monthly time series of water areas for Lakes Wyara and Numalla from March 1987 to December 2021 were obtained from improved monthly water extents in Section 2.2.1. Hypsometric curves describing the relationship between water surface area and level (or elevation) for each lake were derived from the bathymetry heights of a series of the contour lines and the areas enclosed by corresponding contour lines. The hypsometric curves were derived by polynomial regression for the two lakes (see Section 3.2). The monthly time-series of the water surface levels for the two lakes from March 1987 to December 2021 were then produced by interpreting the A-E relationships using the monthly time series of water areas.

Based on developed bathymetric models, we can also calculate the water volumes (or storages) of the two lakes. If we stratify the lake into a sequence of frustums with an equal height interval (Δh), the water volume of the ith frustum can be calculated by the following formula:

$$\Delta V_i = \frac{1}{3}\Delta h \left(A_{i-1} + A_i + \sqrt{A_{i-1} \times A_i} \right) \tag{1}$$

where A_{i-1} and A_i are the base and top surface areas of the frustum respectively.

The lake water volume below (and include) the kth frustum can be calculated by:

$$V_k = \sum_{i=1}^{k} \Delta V_i = \frac{1}{3}\Delta h \sum_{i=1}^{k} \left(A_{i-1} + A_i + \sqrt{A_{i-1} \times A_i} \right) \tag{2}$$

Here, we used height interval of 0.1 m to derive the water surface areas at different water levels from the bathymetry models.

Once calculating the volumes at different water levels, the relationship between water level (or elevation) and volume (or E-V relationship) for each lake can be derived. The time series of the water volumes for the two lakes were then produced by interpreting the *E-V* relationships using the time series of water levels derived in the above steps.

2.2.6. Accuracy assessment and validation

There were no existing bathymetric data and high-accuracy DEMs in the region for accuracy assessment of developed bathymetric models. The ATL08 data acquired in February 2020 (Table. 1) were the only suitable data for accuracy assessment. The terrain heights from the ATL08 data were used as reference data and compared with the corresponding terrain heights extracted from developed bathymetric models to assess the accuracy of bathymetric models. The root mean squire error (RMSE) was calculated for each model by the following formula:

$$RMSE = \sqrt{\frac{\sum_{i=1}^{n} (Hb_i - Hr_i)^2}{n}} \tag{3}$$

where *Hr$_i$ and Hb$_i$* are the reference terrain height from ATL08 and the corresponding terrain height from bathymetric model, and *n* is the number of heights.

There were no gauge observations of water levels available for Lake Wyara and Lake Numalla. Here, the water surface heights from ATL13 data in 2020 and 2021 (Table S1 and Table S2) were used as reference data to validate the time-series of water surface levels for the two lakes. We calculated a mean water surface height of the ATL13 data collected from a RGT on a specific date. The difference between the mean water surface height and corresponding water level on that month from the time-series data was calculated.

3. Results

3.1. Accuracy assessment and validation

The lake terrain heights extracted from developed bathymetric models show high correlations with the reference heights derived from ICESat-2 ATL08 data for both Lake Wyara and Lake Numalla. The coefficient of determination R^2 is greater than 0.997 for both lakes, as seen in Fig. S3. The RMSEs are 0.084 m and 0.112 m respectively, indicating high accuracy of developed bathymetric models. The height differences between water surface levels from time-series and the reference water surface levels derived from ICESat-2 ATL13 range from -0.001 m to -0.100 m for Lake Wyara (Table. S1) and -0.010 m to -0.120 m for Lake Numalla (Table. S2). The average differences of -0.066 m and -0.083 m show time-series of water surface levels derived from this study for both lakes achieved high-accuracy.

3.2. Relationships between inundation frequency and lake terrain height

The relationships between the inundation frequency and lake terrain height for Lakes Wyara and Numalla are illustrated in Fig. S4. The relationships are very well fitted by a biquadratic (or fourth degree) polynomial function for Lake Wyara (Fig. S4a) and best fitted by a cubic polynomial function for Lake Numalla (Fig. S4b). The lake terrain heights derived from the ATL08 data show high correlations with the inundation frequency for both lakes, with the values of coefficient of determination R^2 of 0.989 and 0.993 for Lake Wyara and Lake Numalla respectively as shown in Fig. S4.

3.3. Relationships between water surface area and level

The hypsometric relationships between water surface area and level constructed from the bathymetric models for the two lakes were shown in Fig. S5. Considering the geometric characteristics of the lakes, the A-E relationships were constructed with two hypsometric curves for each of the two lakes due to their flat floors (Fig. 3-4). The A-E relationship for Lake Wyara was fitted by a cubic polynomial function for lower part and a linear function for upper part (Fig. S5a) while the relationship for Lake Numalla was also fitted by two hypsometric curves: the lower part is by a cubic polynomial function; and the upper part is by a biquadratic polynomial function (Fig. S5b). All the hypsometric curves show high correlations between lake water areas and levels with R^2 greater than 0.99.

As the water area of Lake Wyara reaches 30 km² and the water level stands at about 120.3 m, a substantial change emerges. From this point onward, the water level experiences a substantial increase (Fig. S5a) due to the presence of extremely steep banks surrounding the lake (Fig. 4b and c). This momentous change serves as a turning point in the lake's dynamics, where even a minor expansion in water area triggers a considerable surge in the water level. Similarly, Lake Numalla undergoes a comparable pivotal shift. This transformation is characterized by the lake's area reaching 10 km² and the water level attaining an approximate height of 120.7 m (Fig. S5b and Fig. 4e and f). Just like in Lake Wyara, this alteration underscores the interconnected relationship between the lake's expanse and its water level, signifying a turning point in its overall behaviour.

3.4. Lake bathymetric models

The bathymetric models of Lake Wyara and Lake Numalla in the coordinate system of Map Grid Australia 2020 (MGA2020) are shown in Fig. 3a and b respectively. The bathymetric models depict the underwater topography (terrain heights in AHD) and the depths of the lake floors. The depths are measured from the highest shorelines which are defined from the maximum extents of water
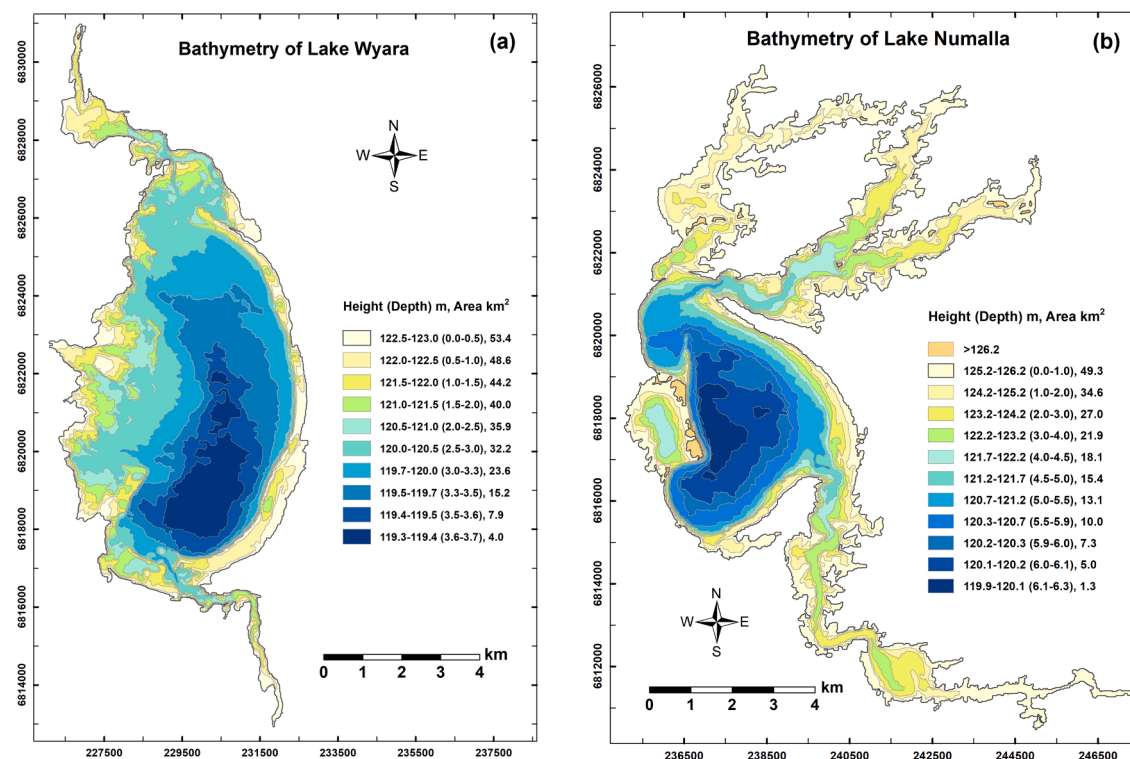

Fig. 3. The bathymetric models of Lake Wyara (a) and Lake Numalla (b) in the coordinate system of Map Grid Australia 2020 (MGA2020), showing terrain height of the lake floor in AHD, depth measured from the highest shoreline (123.0 m for Lake Wyara, and 126.2 m for Lake Numalla), and surface area enclosed by depth contours.
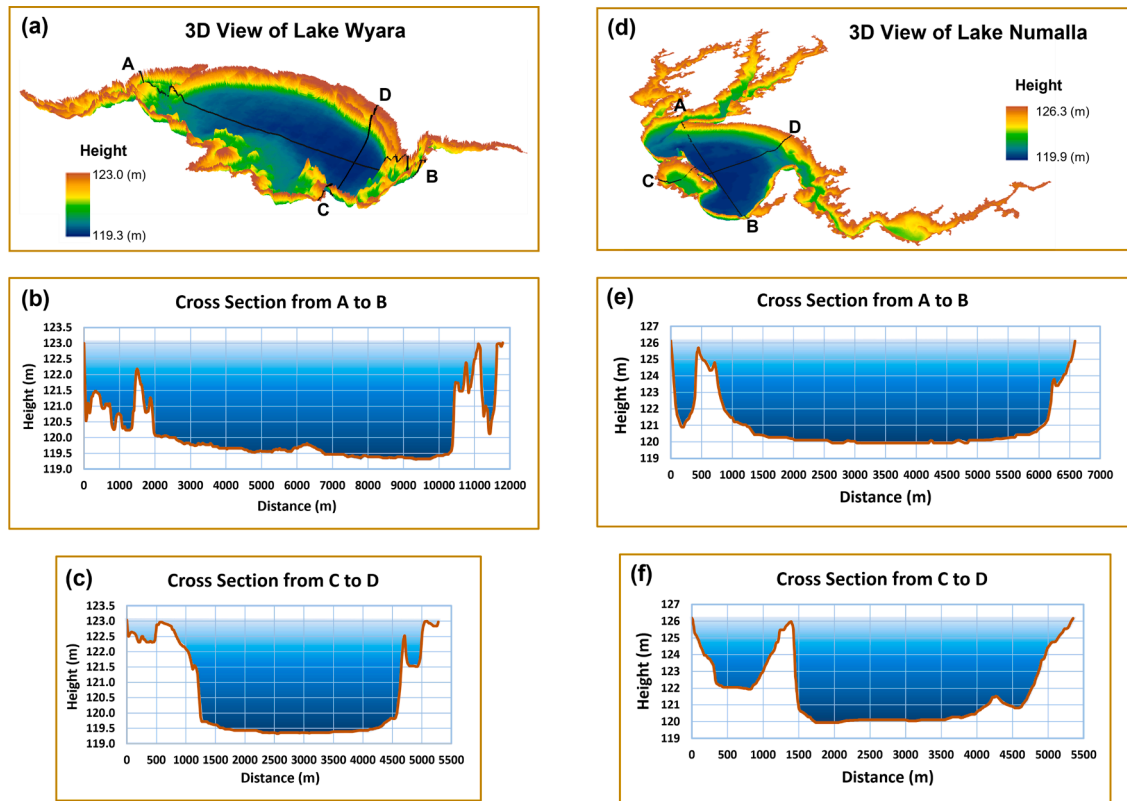
Fig. 4. Cross sections of Lake Wyara (a-c) and Lake Numalla (d-f), including 3D views of the lakes showing the locations of cross sections, cross sections from north to south, and cross sections from west to east.

bodies to the lake floors. The depths of Lake Wyara are measured from 123.0 m height (the outmost contour line) while Lake Numalla from 126.2 m. The surface areas enclosed by depth contours are also shown in Fig. 3a and b. The cross sections from north to south and from west to east which intersect at the deepest locations for Lakes Wyara and Numalla are illustrated in Fig. 4a-c and Fig. 4d-f. The Lake Wyara is D-shaped with the major axis from north to south. The eastern shoreline is smooth and evenly curved while the western shore is irregular with some offshore islands (Timms, 1998). Lake Wyara is about 53.4 km^2 in area (including the lake alone and Werewilka and Kaponyee Creeks) and up to 3.7 m deep when full (Fig. 3a). The lake floor is very flat and slopes slightly from north to south. The deepest area is close to the southern and eastern shores where the banks are steep (Fig. 4b and c). The flatter area with height less than 120.0 m is 23.6 km^2, accounting for 44.2% of the total area of Lake Wyara (Fig. 3a).

Lake Numalla, slightly smaller but much deeper than Lake Wyara, is 49.3 km^2 in area when full, including the main body of the lake, three northwest arms, a long distributary channel of Carwarra Creek to the southeast, and a lakelet to the west of the main body of the lake as shown in Fig. 3b. The lake has a smooth and evenly curved north-eastern shoreline. The lakebed is flattened out (shallower to deeper) from east to west. The western bank adjacent to the lakelet is very steep as shown in Fig. 3b and Fig. 4f. The deepest part of Lake Numalla is located near the western shore of the primary lake area (Fig. 4f) and is up to 6.3 m deep when the lake is full (Fig. 3b). The lake has a flatter floor area of 13.1 km^2 with height less than 121.2 m, accounting for 26.6% of the total area of Lake Numalla (Fig. 3b).

3.5. Dynamics of lake water bodies

Monthly time series of water areas and levels of Lake Wyara and Lake Numalla from May 1987 to December 2021 are shown in Fig. 5 and Fig. 6 respectively. The water levels are referenced to Australian Height Datum (AHD). The figures also illustrate the variances of surface water depths for both lakes. The monthly time series of water volumes in gigalitre (GL) for the two lakes are plotted in Fig. 7. The water areas, levels and volumes of both lakes were highly variable which are closely tied to the climatic conditions of the study area. Monthly rainfall and evaporation over the study area are depicted in Fig. 8. Rainfall contributes directly to the lake water and indirectly through runoff from the surrounding catchment. Evaporation exceeds rainfall in almost every month in this semi-arid climatic region. The maximum water areas and the highest water levels usually occurred in austral summer months from December to February and autumn months from March to May. The variances of lake water bodies displayed a very close resemblance to the changes in rainfall and evaporation. Heavy local rainfall can lead to a rapid increase in water levels. Once they reach their peak, both lakes may sustain this high-water level for several months or even over a year. However, it takes a longer period, sometimes several
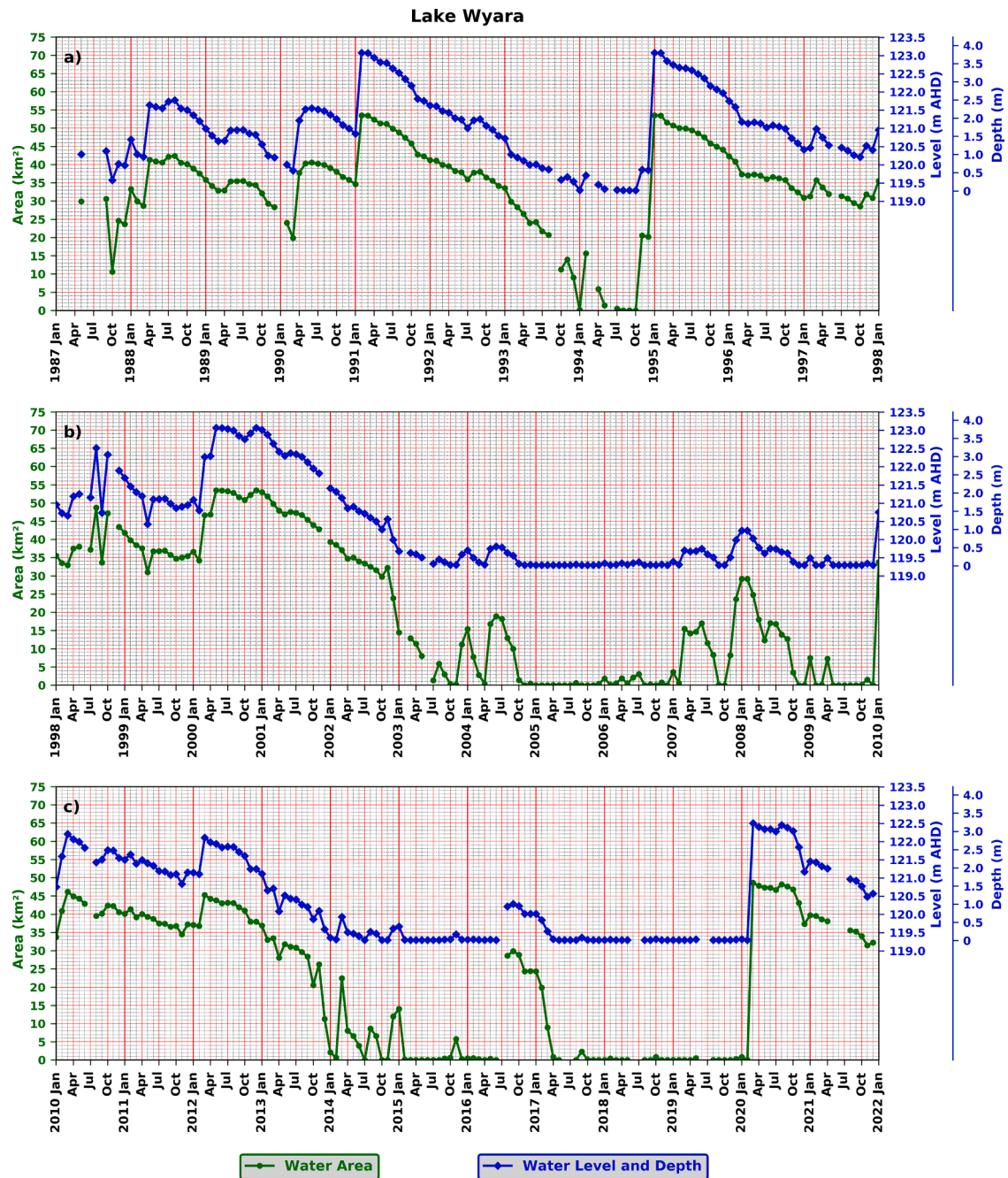
Lake Wyara

Fig. 5. Monthly time series of water area, level, and depth of Lake Wyara over the period of: a) 1987 to 1997, b) 1998 to 2009, and c) 2010 to 2021.

years, for the water levels to recede or for the lakes to dry up. This phenomenon occurs because rainfall is a primary factor contributing to water level fluctuations, while evaporation regulates the water recession in this semi-arid region. For easy visualisation, we present the results in three time periods: 1987 to 1997, 1998 to 2009 and 2010 to 2021. It should be noted that there are some absences of water areas in the time series because of no data in the GSW dataset, resulting in the absences of water levels and volumes as well.

3.5.1. Water dynamics of Lake Wyara

For Lake Wyara between 1987 to 1988, we first saw water level fluctuations between 119.6 m and 120.7 m in 1987 and early 1988 (some data not available in 1987) as shown in Fig. 5a. Because of high rainfall in March, April and July 1988 and low evaporation from April to September 1988 (Fig. 8), the water level was raised to 121.6 m in March 1988 and had been retained at levels above 121.5 m until October 1988 (Fig. 5a). Since then, the lake had generally receded for one and half years until March 1990 when increased rainfall
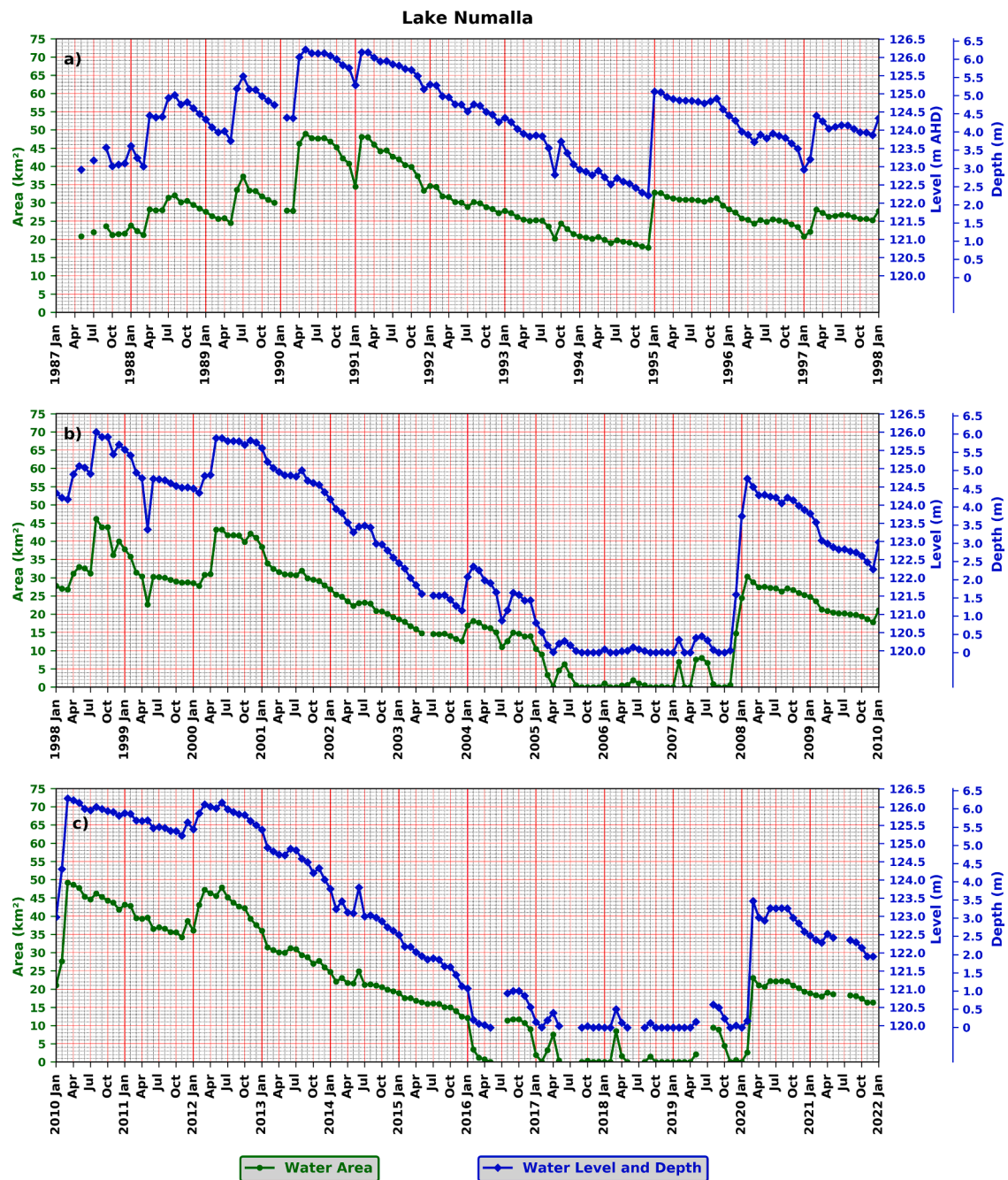
Fig. 6. Monthly time series of water area, level, and depth of Lake Numalla over the period of: a) 1987 to 1997, b) 1998 to 2009, and c) 2010 to 2021.

began to replenish the lake. The water level increased sharply by about 1.5 m to a level of 121.5 m in May 1990. There was then a brief period (about six months) when the water level had been receding until January 1991. Two water level peaks occurred in February 1991 and January 1995 (Fig. 5a) due to high summer rainfall (Fig. 8). The highest water levels of 123.1 m with a depth of 3.9 m were present in February 1991 and January 1995 when water area extended to about 53 km² (Fig. 5a). After the first peak in February 1991, the lake had been receding over the next three years and dried up for most of the time in 1994 owing to long-term rainfall deficiencies during 1991 to 1994 (Fig. 8). After almost one-year dry phase, only within two months, had Lake Wyara once again filled up to the highest water level in January 1995 (Fig. 5a) in the wake of heavy rainfall (Fig. 8).

From 1998 to 2009, Lake Wyara had two major fillings. The first one occurred in late winter and early autumn of 1998 (August to October) with water level fluctuations of about 1.5 m. The second one, caused by high rainfall and low evaporation, began in March
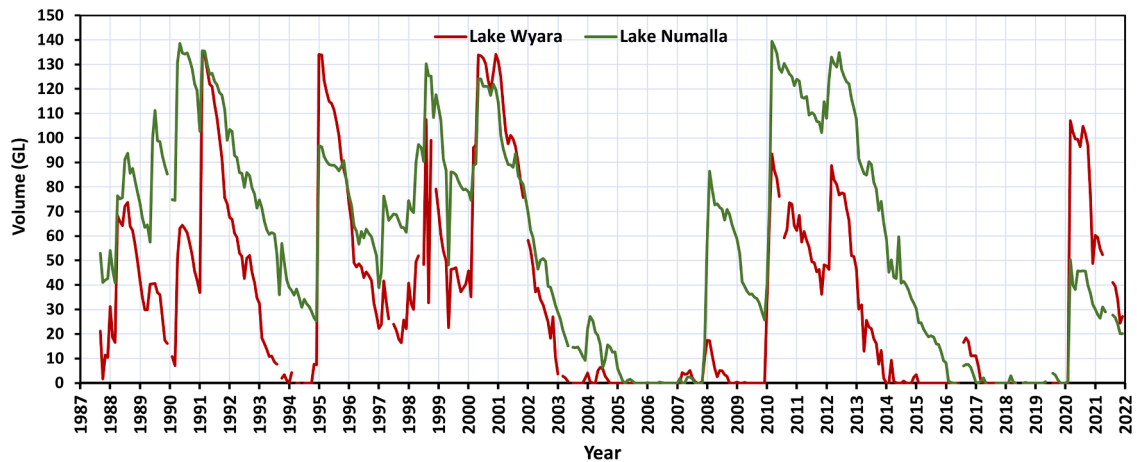
Fig. 7. Monthly time series of water volumes in gigalitre (GL) of a) Lake Wyara (red line), and b) Lake Numalla (green line).
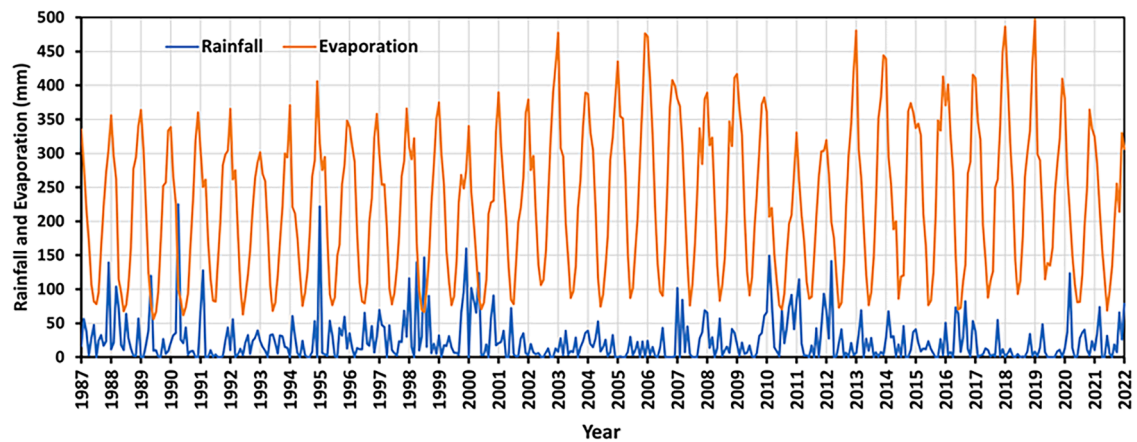

Fig. 8. Local monthly rainfall (blue line) and evaporation (orange line).

2000 and reached the highest level of 123.1 m in May 2000, causing the lake to be inundated up to 53.5 km^2 and 3.8 m deep as illustrated in Fig. 5b. The lake remained at high water levels from May 2000 to February 2001 although there was a brief decrease in September and October 2000. The lake then had a continuous recession over the next two years. This was towards the end of the almost eight-year period of lake inundation (January 1995 to October 2002) when the lake water was consistently deeper than 1 m with an inundated area greater than 30 km^2 except for September and October 1997 (Fig. 5a and b). Lake Wyara was dry or nearly dry from July to November 2003. During the seven years from 2003 to 2009, Lake Wyara was mostly dry due to a combination of low rainfall and high evaporation (as seen in Fig. 8), with only several instances of shallow water with a depth of 0.5 m (apart from a brief inundation from December 2007 to March 2008 caused by summer rains), as depicted in Fig. 5b.

During summer and early autumn in 2010 (January to March), the water level of Lake Wyara had abruptly been elevated to122.2 m in March (Fig. 5c) by heavy rainfall and relatively low evaporation (Fig. 8). The lake had receded in the following two years, but it had retained the water level above 120.8 m with a depth over 1.5 m during this period. In March 2012, higher rainfall and lower evaporation (Fig. 8) led to another rise to a peak level above 122 m, but then decreased continuously over the next two years (Fig. 5c). Lake Wyara dried up in February 2014 and had been mostly dry over the next two and half years although the lake briefly inundated with shallower water on several occasions (Fig. 5c). In September 2016, the water level increased to 120.3 m with a depth of about 1.3 m but declined in subsequent six months, resulting in dry condition which lasted for 34 months from April 2017 to February 2020 (Fig. 5c) because of rainfall deficiencies and very high evaporation as shown in Fig. 8. Heavy rainfall and reduced evaporation in March 2020 (as seen in Fig. 8) swiftly replenished Lake Wyara, leading to an increase in the water area to approximately 48.5 km^2 and a rise in the water level by 3.2 m to reach 122.5 m (Fig. 5c). The lake had retained the high-water level for six months and then began to recede. By the end of 2021, the water area of the lake had decreased to approximately 32 km^2, with a water level of 120.6 m and depth of 1.3 m as shown in Fig. 5c.

3.5.2. Water dynamics of Lake Numalla

Lake Numalla and Lake Wyara showed similar water variation patterns in the time series of water areas and levels over the study period. However, because Lake Numalla is deeper and closer connection to Paroo River than Lake Wyara, it also exhibited its own characteristics in water body dynamics. From 1987 to 1997, for example, the peak water levels occurred at nearly same times for both lakes, but Lake Numalla held water throughout the period although its water level was lower in 1994 when Lake Wyara was completely dried out (Fig. 5a and Fig. 6a). After two major fillings in May 1990 and February 1991, Lake Numalla had undergone four years of substantial reduction in water due to rainfall deficiencies during this period (Fig. 8). The water area decreased from 48 km^2 in February 1991 to 17.5 km^2 in December 1994, with water depth decreasing by about 4 m (Fig. 6a). Heavy rainfall in January 1995 (Fig. 8) significantly filled up the Lake Numalla, with an abrupt increase in water level by nearly 3 m (Fig. 6a). The lake then had two years of continuous reduction in water level until January 1997, followed by an increase in water level by about 1.5 m in March 1997 and a slight decrease for the rest of the year as shown in Fig. 6a.

During the period 1998 to 2010, Lake Numalla experienced two significant fillings due to increased rainfall: one was in August 1998 with a water area of about 46.5 km^2; and the other was in May 2000, covering an area of about 43.5 km^2 (Fig. 6b and Fig. 8). The water level dropped to its lowest point (123.3 m) in May 1999, with a 47.3% decrease in nine months from 46.5 km^2 to 22.5 km^2 (Fig. 6b). Despite two brief rises in water level in 2004, the overall trend of substantial decrease in water body of Lake Numalla had been observed from January 2001 to April 2005 (Fig. 6b) when the region experienced dry conditions, suffering from a prolonged dry spell with severe rainfall deficiencies and high evaporation since middle 2000 (Fig. 8). The lake dried up in April 2005 and had generally been dry until November 2007 as shown in Fig. 6b. Lake Numalla began filling in December 2007 with summer rains (Fig. 8) and filled more than Lake Wyara (Fig. 5b and Fig. 6b), rising by approximately 4.7 m in three months. After this filling, the water level in Lake Numalla declined for two years, dropping over 2.5 m by the end of 2009, but did not dry up completely like Lake Wyara did from November 2008 to December 2009 (Fig. 5b and Fig. 6b).

From 2010 to 2021, Lake Numalla experienced its first major filling in the first quarter of 2010 (Fig. 6c). The lake reached its maximum extent of almost 50 km^2 and highest water level of 126.2 m (6.3 m deep) in March 2010. The water level gradually decreased by about 1 m by November 2011, but returned to a peak level in March 2012, slightly lower than the one in March 2010 (Fig. 6c). Lake Numalla maintained its high water level in the first half of the year 2012 (Fig. 6c) due to abundant rainfall and low evaporation (Fig. 8), but then receded over the next three and half years. The lake had subsequently dried up for four years from February 2016 to February 2020, with only brief inundations (as shown in Fig. 6c) due to rainfall deficiencies and very high evaporation (Fig. 8). The water level abruptly rose by 3. 5 m to 123.45 m in March 2020 (Fig. 6c) because of high rainfall and low evaporation (Fig. 8). The lake then began to recede, reducing to a water level of 121.9 m in December 2021, with an area of about 16 km^2 and depth of 2 m as shown in Fig. 6c.

3.5.3. Variations of lake volumes

The relationships between water surface level and water volume of the two lakes are shown in Fig. S6. The relationships are well fitted by a cubic function for Lake Wyara (Fig. S6a) and a quadratic polynomial function for Lake Numalla (Fig. S6b). Both functions show high correlations between lake water levels and volumes with R^2 greater than 0.999 as shown in Fig. S6. Overall, both Lake Wyara and Lake Numalla exhibited similar variation patterns of water volumes as shown in Fig. 7 which are closely related to the climatic conditions of the region in terms of rainfall and evaporation (Fig. 8). Although Lake Numalla has a smaller surface area than Lake Wyara (Fig. 3a and b), the water volume of Lake Numalla was generally larger than Lake Wyara for most of the times during the study period, retaining water in longer phases than Lake Wyara (Fig. 7). This is because that Lake Numalla lies near the edge of the Paroo floodplain along Boorara Creek and is connected to the Paroo River by a distributary channel of Carwarra Creek (Timms, 2006). As such, Lake Numalla captured water via Carwarra and Boorara Creeks from Paroo River when in flood. The flood water from Paroo River helps maintain the lake's depth. Lake Wyara, on the other hand, is within a virtually closed catchment and fills almost entirely from local catchment although extreme flood overflow from the Paroo River can still affect the lake (Kingsford and Porter, 1994). Therefore, Lake Numalla received water more frequently from Paroo River than Lake Wyara did (Timms, 2006). However, in certain years, such as 1995, 2000, 2001, and 2020, the water volume of Lake Wyara was larger than Lake Numalla (as depicted in Fig. 7). This discrepancy can be attributed to the fact that Lake Wyara has a larger surface area, as illustrated in Fig. 3. Consequently, during years with heavy rainfall, Lake Wyara's greater expanse led to a more substantial increase in its volume compared to Lake Numalla. The largest volumes of Lake Wyara and Lake Numalla occurred in January 1991 and March 2010 with volumes of 132 GL and 140 GL respectively (Fig. 7).

4. Discussion

Spatiotemporal dynamic information on surface water area, level, and volume is a prerequisite for effective wetland conservation and management under the Ramsar Convention (Kingsford et al., 2021; Ramsar Convention on Wetlands, 2018; Rebelo et al., 2018; Xi et al., 2021; Zhang et al., 2022). Lake bathymetry is essential for water dynamic monitoring, wetland conservation, ecohydrological modelling and climate change assessment. However, the lake bathymetric models are usually very difficult to get, especially in data-scarce remote areas. The lack of detailed bathymetric models makes it impossible to provide long-term water dynamic information in support of a wide range of applications. In this study, for the first time, the detailed bathymetric models of Lake Wyara and Lake Numalla were developed by way of leveraging inundation frequency and ICESat-2 photon-counting LiDAR data in semi-arid Australia. The two largest water bodies within the Currawinya Lakes Ramsar site, Lake Numalla and Lake Wyara play an important role in support of an array of native fauna, particularly an abundance and diversity of waterbird species. Some pioneering studies have been done in terms of geomorphology and hydrology of these two lakes (Timms, 1998, 2001, 2006). Timms (1998, 2006) visited Lake

Wyara and Lake Numalla at irregular intervals from 1987 to 2005. On each visit, lake levels were noted. Between visits, information on water levels were obtained from local landowners. The deepest area of Lake Wyara was measured by leveling with a dumpy level when the lake was dry in 1993-1994 (Timms, 1998). Because the two lakes are too big to be mapped efficiently by a dumpy level, only preliminary geomorphic descriptions for these two lakes were obtained from the field inspections along with the study of aerial photos and satellite images (Timms, 1998, 2006). The natural hydrology of the site, in particular, the frequency, duration and timing of inundation of the lakes are generally regarded as the most important underlying process in maintaining the wetlands (NPRSR, 2014). Based on bathymetric models developed in this study, monthly time series of water areas, levels and volumes were derived to describe the long-term (1987-2021) water dynamics of the two lakes. This study provides new insights into the long-term trends of water dynamics of the Ramsar listed lakes in the region. Moreover, with developed hypsometric equations as shown in Fig. S5, scientists and users who are tasked with water management can easily interpret the future dynamic information in water levels of the two Ramsar lakes using monthly water extents in the GSW dataset which will be regularly updated. The outcomes of this study should be of interest to the broader scientific community. The method presented in this study can be adapted to other Ramsar-listed water bodies where bathymetric and water dynamic data have not yet been available.

The method presented in this study offers several distinct advantages when compared to other established techniques. It distinguishes itself through its simplicity and cost-effectiveness, presenting a more economical alternative to methods such as echosounding, SDB, and airborne bathymetric LiDAR. Notably, the datasets utilised in our methodology, namely the GSW dataset and the ICESat-2 photon-counting LiDAR data, are readily accessible at no cost. This accessibility significantly lowers the overall expenditure associated with the development of bathymetric models. Moreover, our method eliminates the necessity for in-situ water depth data, a requirement in traditional SDB methods. This is particularly valuable in regions characterized by data scarcity or remote locations where field measurements may be challenging to obtain. Most importantly, because water occurrence data can effectively capture the entire spectrum of inundation frequency in semi-arid regions, this method proves to be a more suitable choice for constructing lake bathymetric models in semi-arid regions compared to prior research conducted in areas featuring permanent water presence or seldom inundated desert regions. Consequently, our approach addresses a critical need for improved modelling in such regions, where water dynamics are complex and have not been adequately addressed by existing methods. It should be noted that the water dynamic information obtained from this method may be influenced by the temporal resolution (e.g., monthly based water extent) of the GSW dataset derived from Landsat imagery. Additionally, sediment deposition could potentially influence the development of the bathymetric models. Nevertheless, it is worth noting that the use of water occurrence data spanning over three decades may have helped to average out the effects of sediments on the results.

It is also important to acknowledge the limitation regarding the accuracy assessment and validation of results in this study, which is primarily attributed to the unavailability of high-precision Digital Elevation Models (DEM) and water gauge data within the study area. The only available DEM in the study area is the Shuttle Radar Topography Mission (SRTM) DEM, which has a vertical accuracy on the order of several metres (Hirt et al., 2010). Consequently, it cannot be employed for accuracy assessment and validation within the scope of this study. Moreover, due to the limited number of ICESat-2 data, performing cross-validation for the study's results would be inappropriate. Therefore, we opted for a two-step approach for assessment and validation: firstly, the ATL08 terrain data from one reference ground track (Table 1) were used to validate the bathymetric model heights for each lake, and secondly, the water surface heights of ATL13 data from two different years (Table S1 and Table S2) were utilised to validate the water surface levels derived from the bathymetric models of the two lakes.

The Currawinya Lakes are of international significance as part of an inland route for migratory shorebirds from East Asia, providing important summer feeding areas. The unique characteristic features and bathymetric profiles of Lake Wyara and Lake Numalla offer outstanding habitat for a range of important fauna species and for breeding waterbirds. However, the abundance and diversity of waterbird are strongly dependent on the availability of suitable wetland habitats controlled by water surface areas, depths and volumes (BMT WBM, 2009). The regional climate study report indicated that the region would experience significant increase in temperature and prolonged warm spells in the foreseeable future. By 2030, the average annual temperature is expected to surpass the 1986-2005 baseline by 1.7°C. Additionally, annual rainfall is anticipated to decrease by three percent, equivalent to an 11 mm reduction, while annual evaporation is forecasted to increase by approximately three percent, equivalent to an additional 78 mm (State of Queensland, 2019). This study shows that both lakes have undergone significant changes, with a general trend of more frequent and longer period of dry in response to regional climate changes. Low water level and dry periods will result in increase in salinity and decrease in both fish populations and quantities of aquatic plants and invertebrates in the lakes. It will subsequently affect waterbirds population in response to the reduction in food availability at the site. Although both lakes are similar in size and are only about 3 km apart, Lake Wyara is saline and generally clear while Lake Numalla is fresh and turbid (NPRSR, 2014). Our results show that Lake Wyara dried more often than Lake Numalla over the study period. Frequent water dynamics of Lake Wyara resulted in variable salinities ranging from hyposaline conditions as high water levels to hypersaline conditions at low water levels (BMT WBM, 2009). Lake Wyara is an important breeding site for waterbirds such as pelicans and black swans and support huge numbers during breeding periods when water levels are high enough to create breeding islands (BMT WBM, 2009). When Lake Wyara is dry, Lake Numalla would be particularly important for wetland habitats (Kingsford and Porter, 1994). The outcomes of this study provide a touchstone to help understand the historical and ongoing status of Ramsar-listed lakes and contribute to future policy development to withstand the impact of climate change on ecosystem in the region. Due to the limitation of the ICESat-2 data coverage, small lakes, e. g., Kaponyee Lakes, Lake Yumberarra and Lake Karatta in the Currawinya Lakes Ramsar site are not included in this study. However, with the launch of Surface Water and Ocean Topography (SWOT) mission on 16 December 2022 (https://swot.jpl.nasa.gov/), it is possible to use the method developed in this study to model the bathymetry and long-term water dynamics of these smaller lakes.

5. Conclusions

In this study, we leveraged inundation frequency and ICESat-2 photon-counting LiDAR data to create bathymetric models for two Ramsar-listed lakes in a semi-arid area of Australia. This study demonstrated the viability of using our proposed method to generate high-accuracy bathymetric models in a remote area with limited data. Developed bathymetric models were then used to derive the long-term (1987-2021) water dynamics of the two lakes. This is the first time that such a detailed bathymetry and water dynamics analysis has been performed for Ramsar-listed lakes in Australia's Outback region. The results showed that the water areas, levels, and volumes of both lakes were highly variable and closely tied to local climate conditions. Both lakes experienced prolonged dry spells because drought conditions prevailed through much of the 2000s and the 2010s as marked by low rainfall and high evaporation. The dry phases of both lakes in the 2010s became longer than in the 2000s. It highlights the importance of accurate information on lake bathymetry and water dynamics for understanding complex ecological processes and interactions in wetland systems. The findings of this study provide multiple lines of evidence to help understand the historical and ongoing status of Ramsar-listed lakes and contribute to policy development for the resilience of the lakes to withstand the impact of climate change. The method developed in this study has potential applications to other Ramsar-listed bodies where bathymetric and water dynamic data have not yet been available. The outcomes of this study will be beneficial to a wide range of communities for the implementation of Ramsar Convention. It is expected that with the launch of the SWOT satellite, new opportunities have emerged for improved bathymetric and water dynamic modelling of smaller lakes at high spatial and temporal resolution in support of a variety of applications.

Declaration of competing interest

The authors declare that they have no known competing financial interests or personal relationships that could have appeared to influence the work in this paper.

Data availability

Data will be made available on request.

Supplementary materials

Supplementary material associated with this article can be found, in the online version, at doi:10.1016/j.ecohyd.2023.10.003.

References

Abdallah, H., Bailly, J., baghdaji, N.N., Saint-Geours, N., Fabre, F., 2013. Potential of sace-borne LiDAR sensors for global bathymetry in coastal and inland waters. IEEE Journal of Selected Topics in Applied Earth Observations and Remote Sensing 6, 202–216. https://doi.org/10.1109/JSTARs.2012.2209864.

Armon, M., Dente, E., Shmilovitz, Y., Mushkin, A., Cohen, T.J., Morin, E., Enzel, Y., 2020. Determining bathymetry of shallow and ephemeral desert lakes using satellite imagery and altimetry. Geophysical Research Letters 47, e2020GL087367. https://doi.org/10.1029/2020GL087367.

Bacalhau, J.R., Ribeiro Neto, A., Crétaux, J.-F., Bergé-Nguyen, M., Moreira, D.M., 2022. Bathymetry of reservoirs using altimetric data associated to optical images. Advances in Space Research 69, 4098–4110. https://doi.org/10.1016/j.asr.2022.03.011.

Biggs, A.J.W., Bryant, K., Watling, K.M., 2010. Soil chemistry and morphology transects to assist wetland delineation in four semi-arid saline lakes, south-western Queensland. Soil Research 48, 208–220. https://doi.org/10.1071/SR09127.

BMT WBM. (2009). *Ecological Character Description of the Currawinya Lakes Ramsar Site. Prepared for the Queensland Environmental Protection Agency*. Retrieved from Brisbane, Australia.

Cooley, S.W., Ryan, J.C., Smith, L.C., 2021. Human alteration of global surface water storage variability. Nature 591, 78–81. https://doi.org/10.1038/s41586-021-03262-3.

Dörnhöfer, K., Oppelt, N., 2016. Remote sensing for lake research and monitoring – Recent advances. Ecological Indicators 64, 105–122. https://doi.org/10.1016/j.ecolind.2015.12.009.

Fassoni-Andrade, A.C., de Paiva, R.C.D., Rudorff, C.d.M., Barbosa, C.C.F., Novo, E.M.L.d.M., 2020. High-resolution mapping of floodplain topography from space: A case study in the Amazon. Remote Sensing of Environment 251, 112065. https://doi.org/10.1016/j.rse.2020.112065.

Fassoni-Andrade, A.C., de Paiva, R.C.D., Fleischmann, A.S., 2020. Lake topography and active storage from satellite observations of flood frequency. Water Resources Research 56, e2019WR026362. https://doi.org/10.1029/2019WR026362.

Forfinski-Sarkozi, N.A., Parrish, c.E., 2019. Active-passive spaceborne data fusion for mapping nearshore Bathyetry. Photogrammetric Engineering and Remote Sensing 85, 281–295. https://doi.org/10.14358/PERS.85.4.281.

Gao, J., 2009. Bathymetric mapping by means of remote sensing: methods, accuracy and limitation. Progress in Physical Geography 33, 103–116. https://doi.org/10.1177/0309133309105657.

Gorelick, N., Hancher, M., Dixon, M., Ilyushchenko, S., Thau, D., Moore, R., 2017. Google Earth Engine: Planetary-scale geospatial analysis for everyone. Remote Sensing of Environment 202, 18–27. https://doi.org/10.1016/j.rse.2017.06.031.

Heathcote, A.J., del Giorgio, P.A., Prairie, Y.T., 2015. Predicting bathymetric features of lakes from the topography of their surrounding landscape. Canadian Journal of Fisheries and Aquatic Sciences 72, 643–650. https://doi.org/10.1139/cjfas-2014-0392.

Hirt, C., Filmer, M.S., Featherstone, W.E., 2010. Comparison and validation of the recent freely available ASTER-GDEM ver1, SRTM ver4.1 and GEODATA DEM-9S ver3 digital elevation models over Australia. Australian Journal of Earth Sciences 57, 337–347. https://doi.org/10.1080/08120091003677553.

Hodúl, M., Bird, S., Knudby, A., Chénier, R., 2018. Satellite derived photogrammetric bathymetry. ISPRS Journal of Photogrammetry and Remote Sensing 142, 268–277. https://doi.org/10.1016/j.isprsjprs.2018.06.015.

Hollister, J.W., Milstead, W.B., Urrutia, M.A., 2011. Predicting maximum lake depth from surrounding topography. PLos ONE 6, e25764. https://doi.org/10.1371/journal.pone.0025764.

Jasinski, M., Stoll, J., Hancock, D., Robbins, J., Nattala, J., Pavelsky, T., Morrison, J., Jones, B., Ondrusek, M., Parrish, C., the ICESat-2 Science Team, 2021a. Algorithm Theoretical Basis Document (ATBD) for Along Track Inland Surface Water Data, ATL13. NASA Goddard Space Flight Center, Greenbelt, MD. https://doi.org/10.5067/RI5QTGTSVHRZ. Release 5, Release Date August, 2021.

Jasinski, M.F., Stoll, J.D., Hancock, D., Robbins, J., Nattala, J., Morison, J., Jones, B.M., Ondrusek, M.E., Pavelsky, T.M., Parrish, C., Team, T.I.-S., 2021b. ATLAS/ICESat-2 L3A Along Track Inland Surface Water Data, Version 5. NASA National Snow and Ice Data Center Distributed Active Archive Center, Boulder, Colorado USA. https://doi.org/10.5067/ATLAS/ATL13.005.

Jeffrey, S.J., Carter, J.O., Moodie, K.B., Beswick, A.R., 2001. Using spatial interpolation to construct a comprehensive archive of Australian climate data. Environmental Modelling and Software 16, 309–330. https://doi.org/10.1016/S1364-8152(01)00008-1.

Khazaei, B., Read, L.K., Casali, M., Sampson, K.M., Yates, D.N., 2022. GLOBathy, the global lakes bathymetry dataset. Scientific Data 9. https://doi.org/10.1038/s41597-022-01132-9.

Kingsford, R.T., Bino, G., Finlayson, C.M., Falster, D., Fitzsimons, J.A., Gawlik, D.E., Murray, N.J., Grillas, P., Gardner, R.C., Regan, T.J., Roux, D.J., Thomas, R.F., 2021. Ramsar wetlands of international importance - improving conservation outcomes. Frontiers in Environmental Science 9. https://doi.org/10.3389/fenvs.2021.643367.

Kingsford, R.T., Porter, J.L., 1994. Waterbirds on an adjacent freshwater lake and salt lake in arid Australia. Biological Conservation 69, 219–228. https://doi.org/10.1016/0006-3207(94)90063-9.

Kotwicki, V., Allan, R., 1998. La Niña de Australia — contemporary and palaeo-hydrology of Lake Eyre. Palaeogeography, Palaeoclimatology, Palaeoecology 144, 265–280. https://doi.org/10.1016/S0031-0182(98)00122-9.

Leon, J.X., Cohen, T.J., 2012. An improved bathymetric model for the modern and palaeo Lake Eyre. Geomorphology 173-174, 69–79. https://doi.org/10.1016/j.geomorph.2012.05.029.

Li, Y., Gao, H., Allen, G.H., Zhang, Z., 2021. Constructing Reservoir Area–Volume–Elevation Curve from TanDEM-X DEM Data. IEEE Journal of Selected Topics in Applied Earth Observations and Remote Sensing 14, 2249. https://doi.org/10.1109/JSTARS.2021.3051103.

Li, Y., Gao, H., Zhao, G., Tseng, K.-H., 2020. A high-resolution bathymetry dataset for global reservoirs using multisource satellite imagery and altimetry. Remote Sensing of Environment 244, 111831. https://doi.org/10.1016/j.rse.2020.111831.

Liu, K., Song, C., 2022. Modeling lake bathymetry and water storage from DEM data constrained by limited underwater surveys. Journal of Hydrology 604. https://doi.org/10.1016/j.jhydrol.2021.127260.

Mader, D., Richter, K., Westfeld, P., Maas, H.-G., 2021. Potential of a Non-linear Full-Waveform Stacking Technique in Airborne LiDAR Bathymetry. PFG – Journal of Photogrammetry, Remote Sensing and Geoinformation Science 89, 139–158. https://doi.org/10.1007/s41064-021-00147-y.

May, J.-H., May, S.M., Marx, S.K., Cohen, T.J., Schuster, M., Sims, A., 2022. Towards understanding desert shorelines - coastal landforms and dynamics around ephemeral Lake Eyre North, South Australia. Transactions of the Royal Society of South Australia 16, 59–89. https://doi.org/10.1080/03721426.2022.2050506.

Messager, M., Lehner, B., Grill, G., Nedeva, I., Schmitt, O., 2016. Estimating the volume and age of water stored in global lakes using a geo-statistical approach. Nature Communications 7. https://doi.org/10.1038/ncomms13603.

Mishra, V., Cherkauer, K.A., Bowling, L.C., 2010. Parameterization of Lakes and Wetlands for Energy and Water Balance Studies in the Great Lakes Region. Journal of Hydrometeorology 11, 1057–1082. https://doi.org/10.1175/2010JHM1207.1.

Mohammed, I.N., Tarboton, D.G., 2011. On the interaction between bathymetry and climate in the systemdynamics and preferred levels of the Great Salt Lake. Water Resources Research 47, W02525. https://doi.org/10.1029/2010WR009561.

Neuenschwander, A., Pitts, K., 2019. The ATL08 land and vegetation product for the ICESat-2 Mission. Remote Sensing of Environment 221, 247–259. https://doi.org/10.1016/j.rse.2018.11.005.

Neuenschwander, A., Pitts, K., Jelley, B., Robbins, J., Markel, J., Popescu, S., Nelson, R., Harding, D., Pederson, D., Klotz, B., Sheridan, R. (2021a). *ICESat-2 Algorithm Theoretical Basis Document (ATBD) for Land and Vegetation Along-Track Products (ATL08)*. Retrieved from Boulder, Colorado USA: https://nsidc.org/sites/nsidc.org/files/technical-references/ICESat2_ATL08_ATBD_r005.pdf.

Neuenschwander, A.L., Pitts, K.L., Jelley, B.P., Robbins, J., Popescu, S.C., Nelson, R.F., Harding, D., Pederson, D., Sheridan, R., 2021b. ATLAS/ICESat-2 L3A Land and Vegetation Height, Version 5. NASA National Snow and Ice Data Center Distributed Active Archive Center, Boulder, Colorado USA. https://doi.org/10.5067/ATLAS/ATL08.005.

Neumann, T., Brenner, A., Hancock, D., Robbins, J., Saba, J., Harbeck, K., Gibbons, A., Lee, J., Luthcke, S., Rebold, T. (2021a). *ICESat-2 Algorithm Theoretical Basis Document for Global Geolocated Photons (ATL03), Release 005*. Retrieved from Greenbelt, Maryland, USA: https://nsidc.org/sites/nsidc.org/files/technical-references/ICESat2_ATL03_ATBD_r005.pdf.

Neumann, T.A., Brenner, A., Hancock, D., Robbins, J., Saba, J., Harbeck, K., Gibbons, A., Lee, J., Luthcke, S.B., Rebold, T., 2021b. ATLAS/ICESat-2 L2A Global Geolocated Photon Data, Version 5. NASA National Snow and Ice Data Center Distributed Active Archive Center, Boulder, Colorado USA. https://doi.org/10.5067/ATLAS/ATL03.005.

Neumann, T.A., Martino, A.J., Markus, T., Bae, S., Bock, M.R., Brenner, A.C., Brunt, K.M., Cavanaugh, J., Fernandes, S.T., Hancock, D.W., Harbeck, K., Lee, J., Kurtz, N.T., Luers, P.J., Luthcke, S.B., Magruder, L., Pennington, T.A., Ramos-Izquierdo, L., Rebold, T., Skoog, J., Thomas, T.C., 2019. The Ice, Cloud, and Land Elevation Satellite –2 mission: A global geolocated photon product derived from the Advanced Topographic Laser Altimeter System. Remote Sensing of Environment 233. https://doi.org/10.1016/j.rse.2019.111325.

NPRSR. (2014). *Currawinya Lakes Ramsar Site /Currawinya National Park: Ramsar Management Summary 2014*. Retrieved from Brisbane, Queensland, Australia: https://www.awe.gov.au/sites/default/files/documents/currawinya-rms-2014.pdf.

Park, E., Emadzadeh, A., Alcântara, E., Yang, X., Ho, H.L., 2020. Inferring floodplain bathymetry using inundation frequency. Journal of Environmental Management 273, 111138. https://doi.org/10.1016/j.jenvman.2020.111138.

Pekel, J.F., Cottam, A., Gorelick, N., Belward, A.S., 2016. High-resolution mapping of global surface water and its long-term changes. Nature 540, 418–422. https://doi.org/10.1038/nature20584.

Prata, A.J., 1990. Satellite-derived evaporation from Lake Eyre, South Australia. International Journal of Remote Sensing 11, 2051–2068. https://doi.org/10.1080/01431169008955160.

QDEHP. (2014). *Information Sheet on Ramsar Wetlands - Currawinya Lakes*. Retrieved from Brisbane, Australia: http://www.environment.gov.au/water/topics/wetlands/database/pubs/43-ris.pdf.

Ramsar Convention on Wetlands. (2018). *Global wetland outlook: state of the world's wetlands and their services to people*. Retrieved from Gland, Switzerland: https://medwet.org/wp-content/uploads/2018/09/ramsar_gwo_english_web.pdf.

Rebelo, L.-M., Finlayson, C.M., Strauch, A., Rosenqvist, A., Perennou, C., Tøttrup, C., Hilarides, L., Paganini, M., Wielaard, N., Siegert, F., Ballhorn, U., Navratil, P., Franke, J., Davidson, N. (2018). *The use of Earth Observation for wetland inventory, assessment and monitoring: An information source for the Ramsar Convention on Wetlands. Ramsar Technical Report No.10*. Retrieved from Gland, Switzerland: https://www.ramsar.org/sites/default/files/documents/library/rtr10_earth_observation_e.pdf.

Ryan, J.C., Smith, L.C., Cooley, S.W., Pitcher, L.H., Pavelsky, T.M., 2020. Global characterization of inland water reservoirs using ICESat-2 altimetry and climate reanalysis. Geophysical Research Letters 47, e2020GL088543. https://doi.org/10.1029/2020GL088543.

State of Queensland, 2019. Climate Change in the South West Queensland Region. Department of Environment and Science. Retrieved from. https://www.qld.gov.au/__data/assets/pdf_file/0027/68373/south-west-qld-climate-change-impact-summary.pdf.

Timms, B.V., 1998. A study of Lake Wyara, and episodically filled saline lake in southwest Queensland, Australia. International Journal of Salt Lake Research 7, 113–132. https://doi.org/10.1007/BF02441882.

Timms, B.V., 2001. A study of the Werewilka Inlet of the saline Lake Wyara, Australia – a harbour of biodiversity for a sea of simplicity. Hydrobiologia 466, 245–254. https://doi.org/10.1023/A:1014597131801.

Timms, B.V., 2006. The geomorphology and hydrology of saline lakes of the middle Paroo, arid-zone Australia. Proceedings of the Linnean Society of NSW 127, 157–174.

Xi, Y., Peng, S., Ciais, P., Chen, Y., 2021. Future impacts of climate change on inland Ramsar wetlands. Nature Climate Change 11, 45–51. https://doi.org/10.1038/s41558-020-00942-2.

Xu, N., Ma, Y., Zhou, H., Zhang, W., Zhang, Z., Wang, X.H., 2022. A method to derive bathymetry for dynamic water bodies using ICESat-2 and GSWD data sets. IEEE Geoscience and Remote Sensing Letters 19, 1–5. https://doi.org/10.1109/LGRS.2020.3019396.

Zhang, Z., Liu, X., Wright, W., 2022. Spatiotemporal water dynamic modelling of Ramsar-listed lakes on the Victorian Volcanic Plains using Landsat, ICESat-2 and airborne LiDAR data. Ecological Informatics 71, 101789. https://doi.org/10.1016/j.ecoinf.2022.101789.

Zhao, G., Gao, H., 2018. Automatic correction of contaminated images for assessment of reservoir surface area dynamics. Geophysical Research Letters 45, 6092–6099. https://doi.org/10.1029/2018GL078343.